

COMMON SCATTER POINT DATA MAPPING

S. Dell, D. Gajewski, and C. Vanelle

email: *sergius.dell@zmaw.de*

keywords: *Data mapping, migration velocity analysis, time imaging*

ABSTRACT

CSP data mapping is a tool in seismic-reflection imaging which allows to generate common scatter-point (CSP) gathers from common midpoint (CMP) data. A CSP gather is similar to a CMP gather, however the move out is based on the distance from the sources and receiver to the scatter point location. The CSP gather as well as the CMP gather is focused by NMO and stacking. The CSP stack is a complete Kirchhoff prestack migration section, while the CMP stack still requires poststack migration.

A key concept of the method is the parameterization of the double square root (DSR) equation into the apex time. The parameterized migration operator allows to map the summed amplitude directly into the apex of the travelttime surface. Also the algorithm is formulated in the space-time domain, which enables prestack migration velocity analysis and multiparameter stacking like the Common Reflection Surface (CRS) stack. The possibility to regularize the CSP gather in the data mapping process and the absence of the diffractions enables a more accurate velocity analysis. The multiparameter stacking of CSP gathers using, e.g. the CMP or the CRS stacking provides enhanced image as compared to the PreSTM.

Application to a complex synthetic model and field data demonstrate that the method is stable and produces highly focused time migrated images.

INTRODUCTION

Prestack time migration (PreSTM) still represents the majority of seismic imaging activities in the industry. The reason for this is the speed and robustness of time imaging and its ability to focus seismic events for most geological settings. One of the preferred PreSTM methods is the common offset (CO) Kirchhoff diffraction stack. The time image of the seismic wavefield is steered by a migration operator based on the double-square-root (DSR) equation (Yilmaz and Claerbout, 1980). For every CO section the summed amplitude is assigned to the zero offset (ZO) apex of the migration operator. When the velocity model is correct, the PreSTM leads to flat image gathers. Although the PreSTM provides enhanced images, migrated seismic data are not suitable for the further applications like stacking velocity analysis or multiparameter stack.

There exist several methods to overcome this limitation to use the seismic data after the PreSTM. Bancroft et al. (1998) proposed to construct the CSP gathers using the equivalent offset. A CSP gather is similar to a CMP gather, however the move out is based on the distance from the sources and receiver to the scatter point location. The CSP gather is focused by NMO and stacking and the CSP stack is a complete Kirchhoff prestack migration section. The equivalent offset method is based on a reformulation of the DSR operator into a single square root. The single square root uses an equivalent offset representing the the surface distance from the scatterpoint to a collocated source and receiver. Silva and Wang (2002) proposed to build velocity models and to image seismic data after PreSTM. Their method is based on the separation of the DSR equation into velocity-dependent and velocity-independent terms. The velocity-dependent term is the hyperbolic NMO correction. In the PreSTM this corresponds to the application of a vertical correction of

the initial migration velocity model.

We introduce a new method, which we call CSP data mapping, that generates CSP gathers from input CMP gathers. The developed method is based on the parameterization of the DSR equation into apex time and allows in every CO section to map the summed amplitude directly into the corresponding CO apex of the migration operator. The output CSP gathers have the same offset size as the input CMP gathers and are suitable for migration velocity analysis and stacking. We then perform imaging with the CSP gathers using the CRS stack. The CRS stack is a multiparameter stack that is based on a second-order approximation of the kinematic reflection response of a reflector segment in depth. We demonstrate by complex synthetic data and field data, that the CRS stack of the CSP gathers provides more focused migrated images than the conventional PreSTM.

THEORY

Kirchhoff Diffraction Stack

The Kirchhoff diffraction stack belongs to the seismic time migration methods, that remove the influence of the overburden from the data. In detail, migration alters the location and inclination of reflection events, collapses diffraction patterns that are caused by scatter points and unfolds triplications. The time migrated section is constructed in the time domain and assumes hyperbolic move out of the reflection events. An appropriate velocity model is essential and usually root mean square (RMS) velocities serves as time migration velocities. Generally, the Kirchhoff diffraction stack is based on the fact that the diffraction traveltime surface or Huygens surface t_D of an actual reflection point M_R and the reflection traveltime surface t_R are tangent in the time domain at the stationary point N_R (Fig. 1). In the same way, the isochron of a reflection event N_R and the reflector are tangent at M_R in the depth domain. These tangency conditions were first observed by Hagedoorn (Hagedoorn, 1954) and are commonly referred to as Hagedoorn's imaging condition or dualities (Schleicher et al., 2007). The main idea of Kirchhoff migration is to treat each point of a

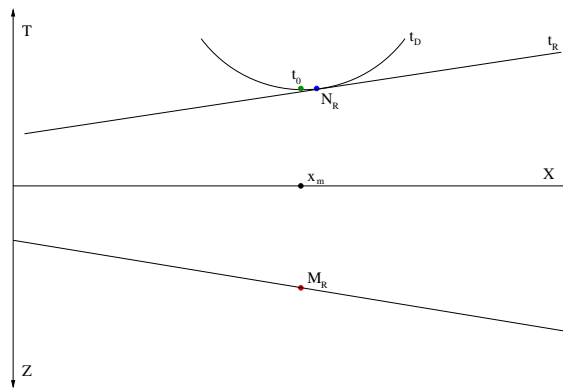


Figure 1: Hagedoorn's imaging condition. The Huygens curve $t_D(M_R)$ of a reflection point M_R is tangent to the reflection traveltime curve $t_R(N_R)$ at point N_R in the time domain.

sufficiently dense grid in the considered target area as a potential diffraction point. The Huygens curve can be calculated independently for any of these points from the image time associated with the actual depth location for a particular migration operator using the known velocity model. The migration operator is given by the double square root equation

$$t_D = \sqrt{\frac{t_0^2}{4} + \frac{(m-h)^2}{v^2}} + \sqrt{\frac{t_0^2}{4} + \frac{(m+h)^2}{v^2}} \quad (1)$$

where h is half source-receiver offset, t_0 is the image time, m is the midpoint displacement with respect to the considered CMP position m_0 and v is the migration velocity. As the image time is generally not known, the migration output is assigned to the ZO operator apex. In case of CO prestack migration, the procedure is carried out for each individual offset (Spinner, 2007).

In the time migration process, the seismic amplitudes along the Huygens curve are summed up and the result is assigned to the corresponding ZO apex time. If the diffraction traveltime curve is tangent to the reflection traveltime curve for an actual reflection point, the summation along the diffraction curve leads to a nonnegligible result due to constructive interference. Otherwise, the contribution ideally yields zero.

Common Scatterpoint Gather

The traveltime surface of a single scatter point at (m_0, t_0) is given by the DSR equation (Eq. 1) and is known as the Cheops pyramid (Claerbout, 1985). A CSP gather building process can be defined as a collection of energy from all input traces in 3-D space of midpoint, offset and time (m, h, t) within the migration aperture (Fig. 2a) and the recollection of their energy in a 2-D space of offset and time (h, t) along a path (Fig. 2b). A CMP gather that is located at the scatter point (m_0) intersects the Cheops pyramid on a hyperbolic path, which coincides with the apexes of the traveltime surface (Fig. 2, 250. CMP). For this CMP all the scattered energy will be focused along the hyperbolic path (Fig. 2b). The intersections of all other CMP gathers have nonhyperbolic paths. For these CMP all the scattered energy will be mispositioned.

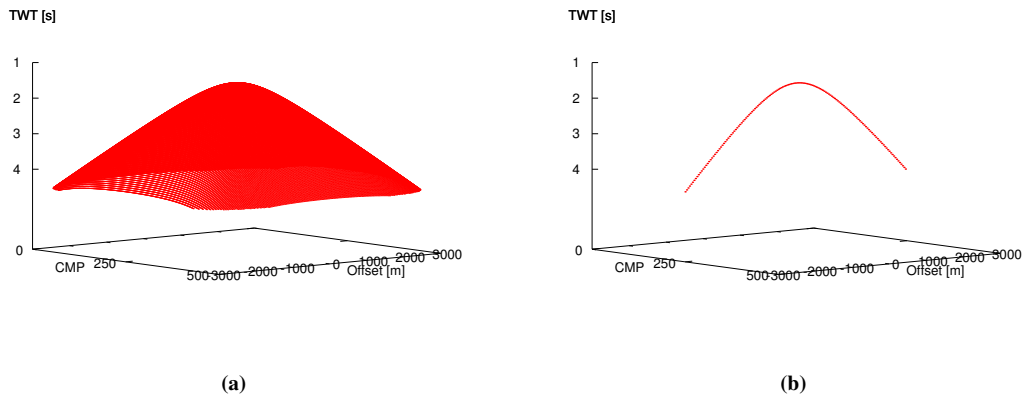


Figure 2: The traveltime surface $t(m, h)$ for a single scatter point (a). The traveltime surface is known as the Cheops pyramid. The CSP gather formed by collapsing the Cheops pyramid to a hyperbola in the $m = 0$ plane. The apex of the hyperbola lays at (m_0, t_0) .

Similar to the traveltime expression for the CMP gather, the traveltime in the CSP gather can be evaluated as a Taylor expansion. The move out in the CSP gather is based on the distance from the sources and receivers to the scatter point location. The ZO ray of the CSP gather coincides with the image ray. Due to this the traveltime is expanded in the vicinity of the image time. Truncation after the second term, the traveltime of the CSP gather is given by

$$t^2 = t_0^2 + \frac{4h^2}{v_m^2}$$

where t_0 is the image time, h is half source-receiver offset and v_m is the migration velocity.

Migration velocity

Since time migration as well as data mapping is based on the Kirchhoff's approach, the well defined migration velocity model is necessary. Usually the migration velocities are determined from root mean square (RMS) velocities. However, the RMS velocity is not known and is approximated by stacking velocity v_{stk} which then serves as migration velocity. The stacking velocity is attached to the stationary point of the migration operator, but the migration velocity is defined at the apex of the migration operator. Due to this the time migration velocity v_c may deviate from the stacking velocity, e.g., in case of dipping reflectors. The migration velocity v_c is not a physical property and can rather be interpreted as a best fit parameter

which fit the migration operator to the reflection events in the data. In order to correct for the difference between v_c and v_{stk} the velocity model needs to be refined. Conventionally residual moveout analysis (RMO) is carried out to refine time migration velocities (Yilmaz, 2001). The RMO routine is an iterative approach and starts with PreSTM which is performed with an initial velocity model. After the PreSTM image gathers are constructed which may show residual moveout. For the selected image gathers an inverse NMO correction is applied using the initial velocities. The inverse NMO correction forms CSP gathers from the image gathers. However, the RMO algorithm makes the assumption that a location of the output CSP gather coincides with a location of the input CMP gather. In the case of lateral velocity variations this assumption is not valid and the RMO algorithm forms the CSP gathers with the wrong velocities. After the CSP gathers have been formed, they enter into a classical stacking velocity analysis. Stacking velocity analysis of CSP gathers matches the observed traveltime with the migrated output traveltime and is based on the distances from the sources and receivers to the CSP location and not on the source-receiver offset as for velocity analysis of the CMP gathers (Bancroft et al., 1998). There is no reflection point smearing as in the CMP gathers for the dipping reflector. Due to increased reflector resolution of the CSP gather, a more accurate velocity model may be estimated from the CSP gathers. Even in the case of the mild lateral velocity variation the stacking velocity analysis in the CSP gathers provides proper migration velocities. As the velocity analysis is usually carried out on a coarse grid, the velocities have to be interpolated onto the migration grid. Eventually the interpolated stacking velocities build an updated migration velocity model.

Data mapping

The principle of the PreSTM is to assign the migration output to the ZO apex of the migration operator, while the principle of the CSP data mapping is to assign the migration output to the CO apex of the migration operator given by

$$t_{apex} = \sqrt{t_0^2 + \frac{4h^2}{v^2}} \quad (2)$$

where t_0 is the image time that corresponds to the ZO operator apex, h is half source-receiver offset and v is the migration velocity. Fig. 3 shows the principle of the time migration and the data mapping. The

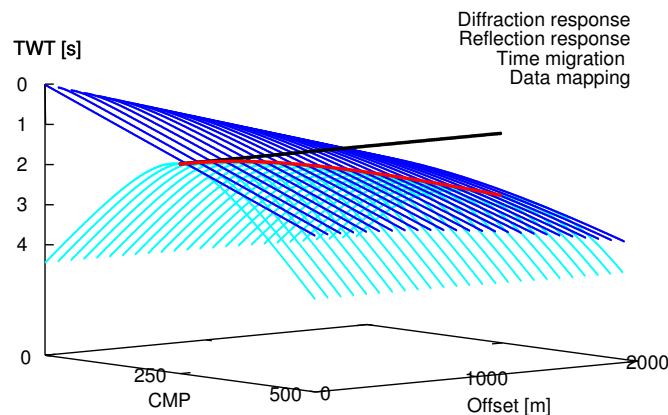


Figure 3: The figure compares the principle of time migration and data mapping for a homogeneous model with a dipping reflector. The reflection response is depicted in blue. The migration operator for CMP 250 is depicted in cyan. The migration output is assigned to the ZO operator apex for every CO section (black line). The mapped output is assigned to the CO operator apex for every CO section (red line).

diffraction traveltme curve defined by the DSR formula (Eq. 1) can be parameterized with the CO apex time t_{apex} (Eq. 2).

$$t = \sqrt{\frac{t_0^2}{4} + \frac{m^2 - 2mh + h^2}{v^2}} + \sqrt{\frac{t_0^2}{4} + \frac{m^2 + 2mh + h^2}{v^2}}$$

$$t = \sqrt{\frac{t_0^2}{4} + \frac{h^2}{v^2} + \frac{m^2 - 2mh}{v^2}} + \sqrt{\frac{t_0^2}{4} + \frac{h^2}{v^2} + \frac{m^2 + 2mh}{v^2}}$$

$$t = \sqrt{\frac{1}{4} \left(t_0^2 + \frac{4h^2}{v^2} \right) + \frac{m(m-2h)}{v^2}} + \sqrt{\frac{1}{4} \left(t_0^2 + \frac{4h^2}{v^2} \right) + \frac{m(m+2h)}{v^2}}$$

With equation 2 one obtains:

$$t = \sqrt{\frac{t_{apex}^2}{4} + \frac{m(m-2h)}{v^2}} + \sqrt{\frac{t_{apex}^2}{4} + \frac{m(m+2h)}{v^2}} \quad (3)$$

Please note, that the velocity in the latter equation is parameterized for the CO apex time t_{apex} but belongs to ZO apex time of the migration operator t_0 . Thus the parameterized DSR equation finally is

$$t = \sqrt{\frac{t_{apex}^2}{4} + \frac{m(m-2h)}{v(t_0)^2}} + \sqrt{\frac{t_{apex}^2}{4} + \frac{m(m+2h)}{v(t_0)^2}} \quad (4)$$

To find the velocity $v(t_0)$, which corresponds to t_{apex} a search procedure is performed (Fig. 4). A similar procedure is also applied for the generation of CRS Supergather (Baykulov and Gajewski, 2009). All t_0 traveltimes within the time window $[0; t]$ and a range of velocities $[v_{min}, v_{max}]$ are tested for an event $A(t_A, h_A)$ to determine the best fitting hyperbola. The hyperbolas are computed using the equation for CO operator apex (Eq. 2). After the time t'_0 which corresponds to the minimum deviation between the computed and the actual time for sample $A(t_A, h_A)$ is found, velocity belonging to t_0 is determined.

The CSP data mapping forms the CSP gathers directly from the input CMP gathers with initial velocities.

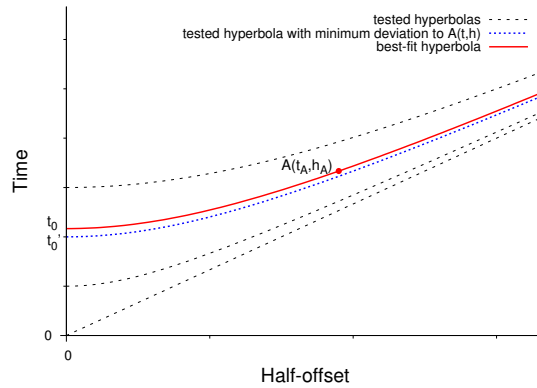


Figure 4: Testing traveltme curves to find the best-fit hyperbola for the sample $A(t_A, h_A)$. The sample $A(t_A, h_A)$ corresponds to an apex of the CO migration operator. All t_0 traveltimes within the time window $[0; t]$ and a range of velocities are tested. The time t'_0 corresponds to the minimum deviation between the computed and the actual time for sample $A(t_A, h_A)$. This time is assumed to be the searched for ZO apex time. The velocity corresponding to this time is then assumed to be the searched for $v(t_0)$ velocity. The tic interval of the TWT axis corresponds to the time sample rate of the data.

As the initial velocities we use the stacking velocities that are obtained as a byproduct after an automatic CMP stack of the CMP gathers. The whole process is performed automatically and doesn't require the manual picking of the velocities. Neither inverse NMO correction nor velocity interpolation on the migration grid is necessary. Thus the generation of the CSP gathers with the CSP data mapping is more reliable than with the RMO method. In comparison to the equivalent offset method the CSP data mapping generates

CSP gathers that doesn't exceed the size of the input CMP gathers in the offset direction. The enlarged size of the CSP gathers in equivalent offset method may lead to the violation of the hyperbolic approach. In this case not all traces are accounted for the stacking velocity. After the CSP gathers have been formed with the initial stacking velocities, they enter into the automatic CRS stack.

RESULT

In order to demonstrate the potential of the developed data mapping, it is applied to synthetic and field data.

Synthetic data

Sigsbee2a Figure 5 shows the stacked section of the full wavefield for the synthetic Sigsbee2a model. Sigsbee 2A is a synthetic constant density acoustic data set released in 2001 by the "SMAART JV" consortium. Sigsbee2A models the geologic setting of the Sigsbee escarpment in the deep water Gulf of Mexico. Irregular boundaries of the salt body cause strong diffractions in the right part of the section. In the left part of the section diffractions are caused by scatter points.

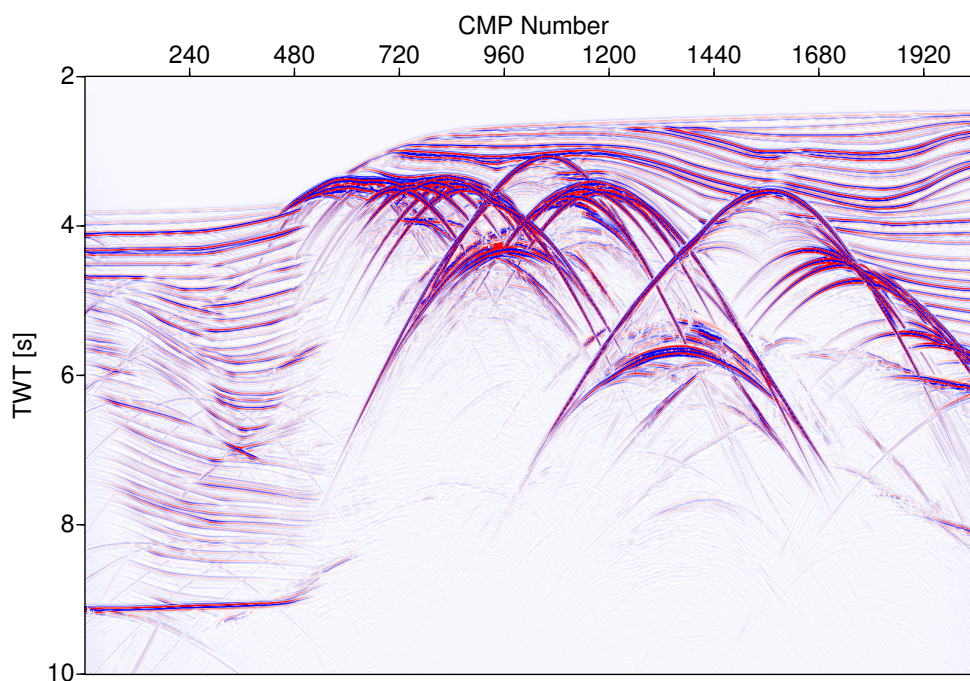


Figure 5: Automatic CRS stack of Sigsbee2a

Figure 6 shows the CMP gather (a), the corresponding CSP gather (b) and their velocity spectra (c,d). When a scatter point is located at the considered output position m_0 of a CSP gather the scattered energy is constructively stacked along the hyperbolic paths in the CSP gather. The energy from scatter points displaced from the output position m_0 is canceled by a destructive interference. Velocity analysis of CSP gathers and of CMP gathers was done using a conventional semblance technique. Due to the regular geometry of the CSP gathers and the absence of diffractions the velocity resolution is improved. Figure 7 shows the prestack time migrated section and CRS stack section of CSP gathers. Time migration velocities were obtained from the interval velocities by Dix inversion. The data mapping as well as the time migration were performed with the same velocity model. For the CSP gathers an automatic CRS stack was performed.

In the stack section the reflections appear more continuous compared to the CMP prestack time migrated section.

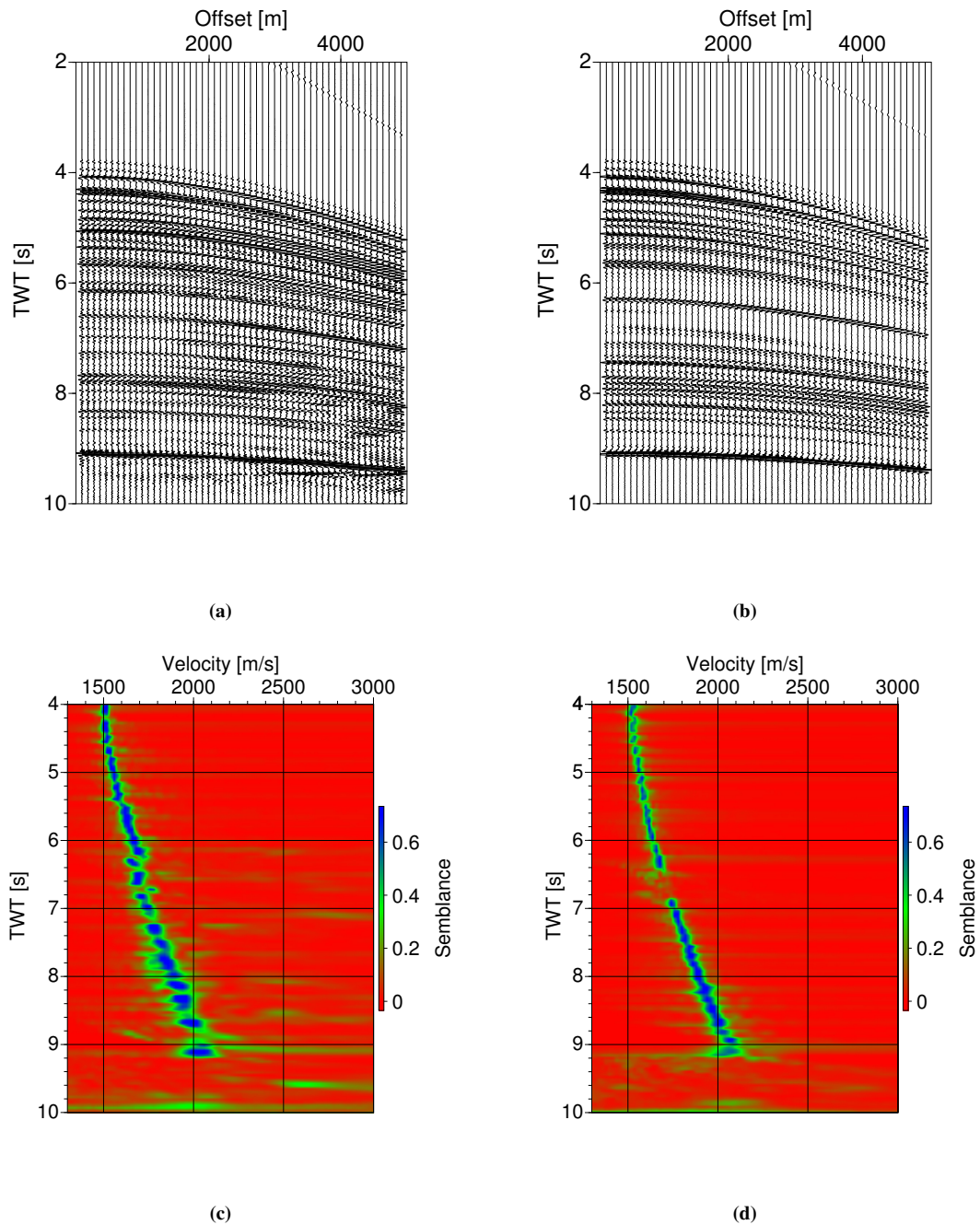
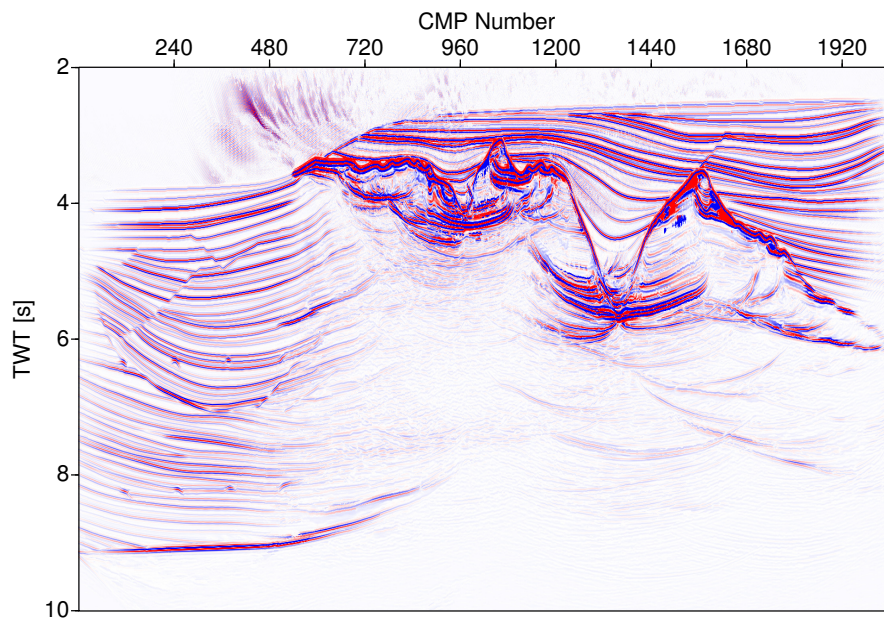
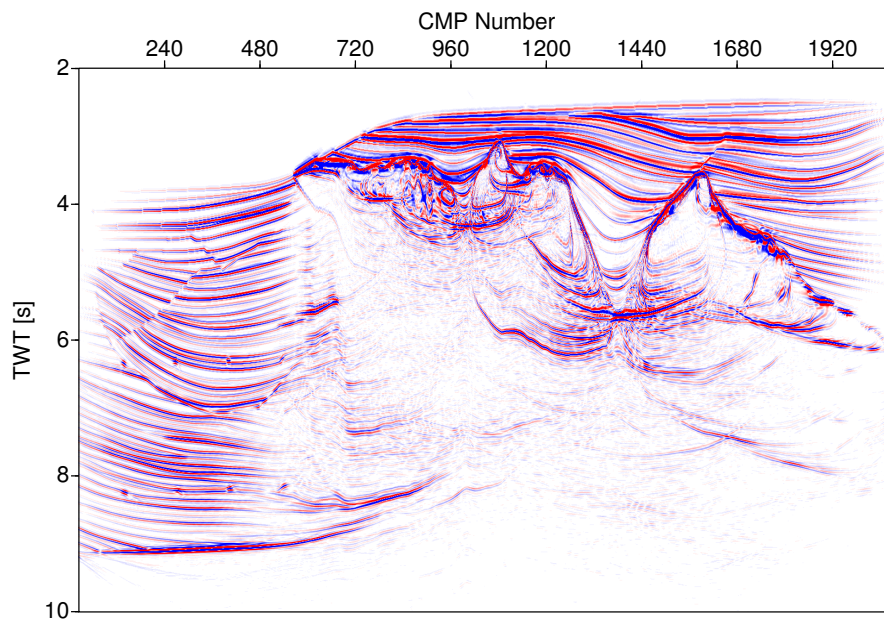


Figure 6: CMP gather (a) and corresponding CSP gather (b) for the Sigsbee2a model. Velocity spectra of CMP (c) and of CSP gathers (d). The spectrum of the CSP gather is better focused and has higher semblance values.



(a)



(b)

Figure 7: Sigsbee2a model. Automatic CRS stack of the mapped data (b) and prestack time migrated section (a). Reflections appear more continuous and the salt-sediment boundaries are easier to identify in the CRS stack section of the CSP gathers compared to the prestack time migrated section.

Field data

Marine data from the Levantine Basin The data set from the central Levantine Basin in the south-eastern Mediterranean Sea covers the basinal succession of the Messinian Evaporites, the Pliocene-Quaternary overburden, and the upper pre-Messinian succession. According to the chronostratigraphic scheme the precipitation of the basinal succession started around ~ 5.6 mya during the Messinian Salinity Crisis (Clauzon et al., 1996). The Levantine Basin has a complex seismic stratigraphy of the basinal succession (Netzeband et al., 2006). The deformation pattern of the intra-evaporite sequences include folds and thrust faulting, which gives evidence for extensive salt tectonics and shortening during the depositional phase. Post-depositional gravity gliding caused salt rollers in the extensional marginal domain, compressional folds, and faults within the Levantine basin. A part of the data consisting of 2000 CMP gathers with a total line length of ~ 15 km was chosen for the processing. 2D acquisition was performed, with a shot spacing of 25 m and a receiver spacing of 12.5 m, with maximum offsets of 7325 m. The record length was 8 s with 4 ms sample rate.

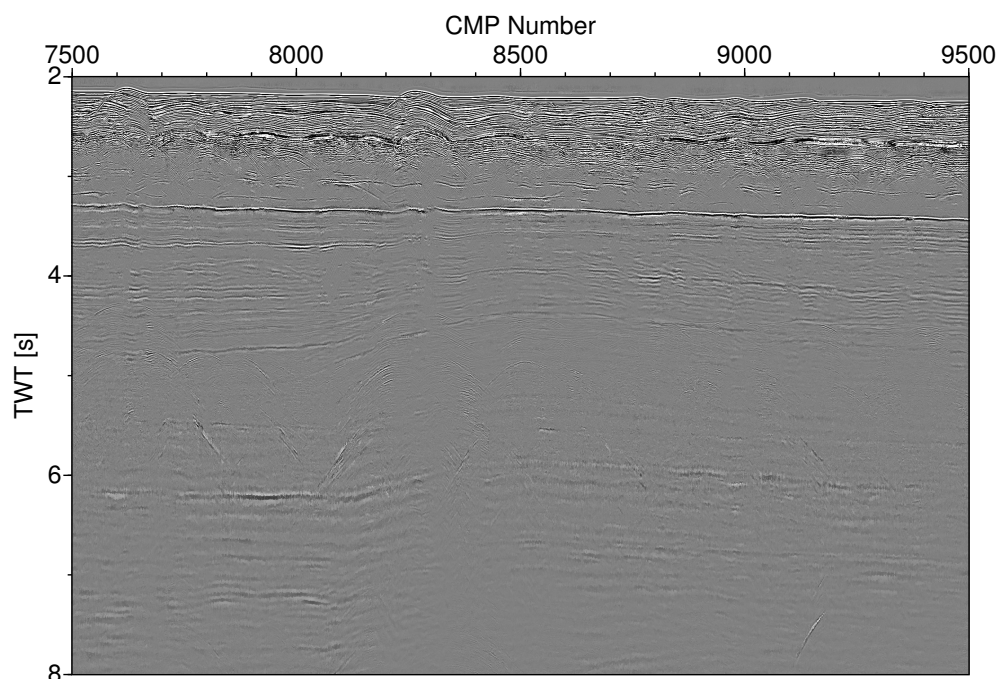


Figure 8: Marine data from the Levantine Basin, automatic CRS stack.

Figure 9 shows the CMP gather (a), the corresponding CSP gather (b) and their velocity spectra (c,d). As migration velocities we used stacking velocities provided by TGS-TOPEC. The CSP data mapping as well as the time migration was performed with the same velocity model. When scatter points are located at the output position of a CSP gather the scattered energy is constructively stacked along hyperbolic paths in the gather. The energy from scatter points displaced from the output location is canceled because of destructive interference. Velocity analysis of CSP and of CMP gathers was performed by conventional semblance technique. Due to the regular geometry of the CSP gathers and the absence of diffractions the velocity resolution is improved. For the CSP gathers an automatic CRS stack was performed. Figure 10 shows the prestack time migrated section (b) and CRS stack of CSP gathers (d). The reflections appear more continuous and faults and subsalt structures more crisp in the latter section compared to the CMP

prestack time migrated section.

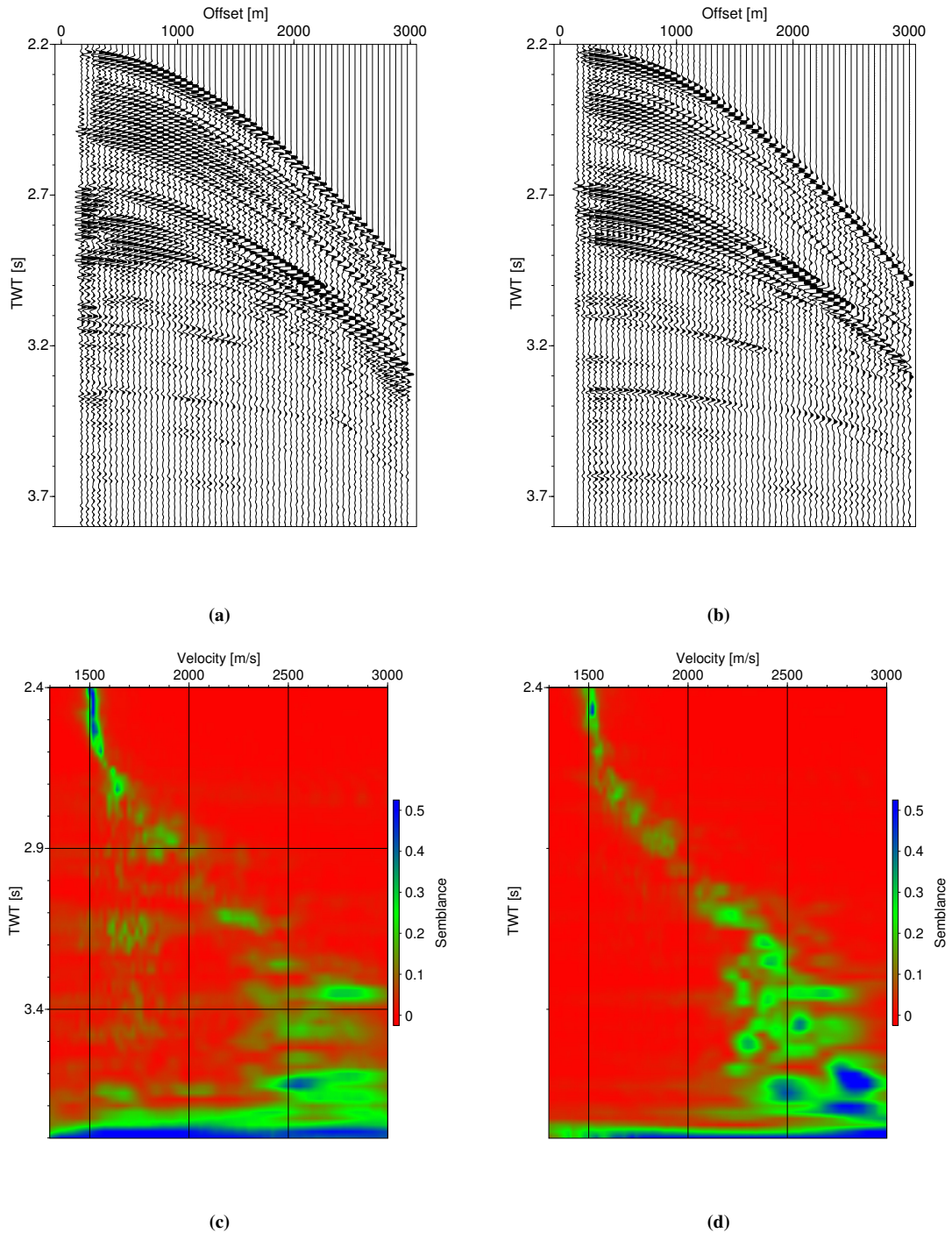
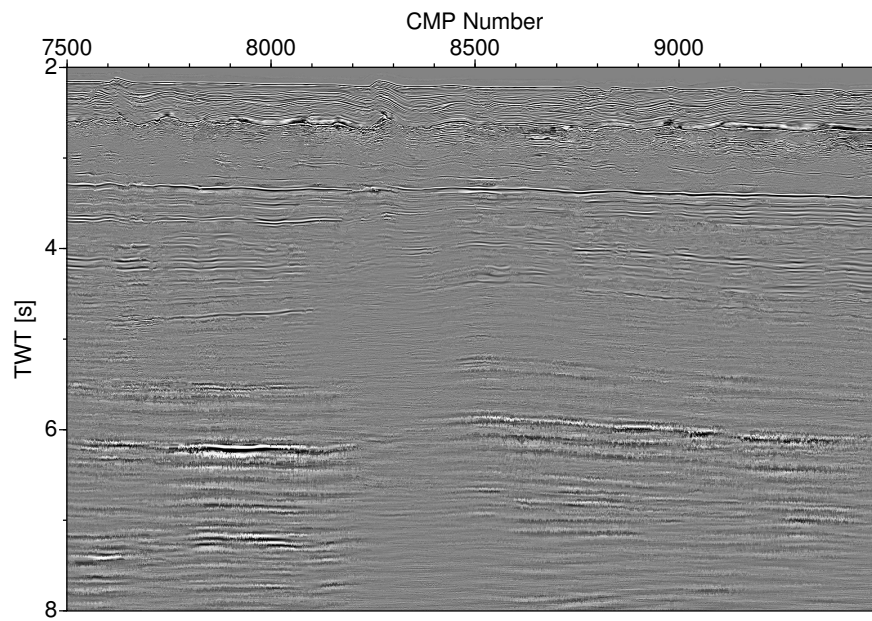
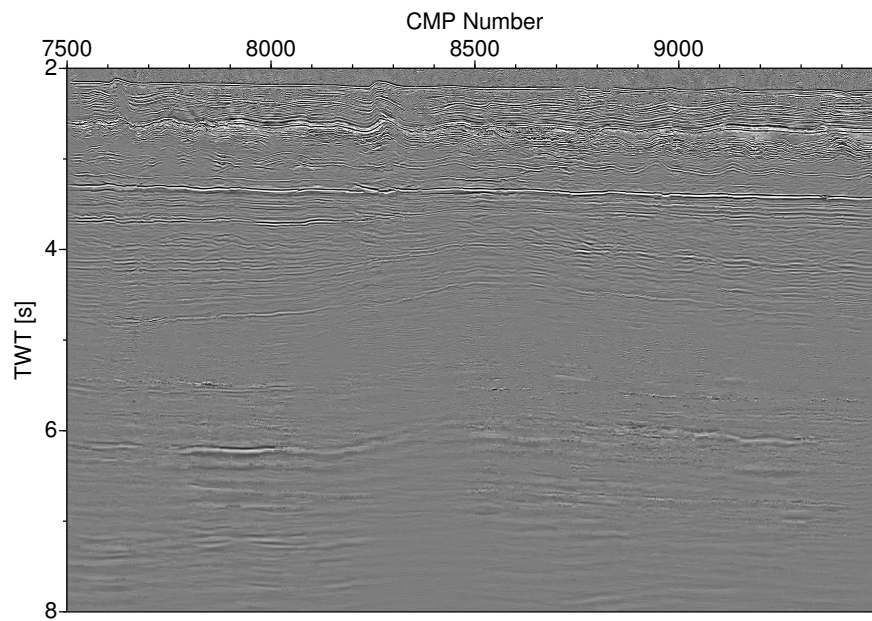


Figure 9: Marine data from the Levantine Basin. CMP gather (a) and corresponding CSP gather (b). Velocity spectra of the CMP gather (c) and of the CSP gather (d). The latter is better focused and provides higher semblance values.



(a)



(b)

Figure 10: Marine data from the Levantine Basin. Automatic CRS stack of the mapped data (b) and prestack time migrated section (a). Reflections appear more continuous and the faults are easier to identify in the CRS stack section of the CSP gathers compared to the time migrated section.

Marine data from the North Sea The study area is located in the North Sea close to the German coast line. Salt structures and complex fault systems characterize the region. The area is a part of the intracratonic Southern Permian Basin formed at the end of the Variscan orogeny. The orogeny occurred in Paleozoic times (from ~ 390 to ~ 310 mya). It reflects the continental collision between Laurasia and Gondwana to form the supercontinent of Pangea (Mohr et al., 2005). The sedimentation process started in the Upper Rotliegend and continued to the evaporites of the Zechstein Group, which reached up to 800 m in thickness. Different phases of salt movements that started in Triassic time formed the salt structures of the region. Each phase is characterized by changing tectonic regimes and different kinds of salt diapirism. A part of the data consisting of 2000 CMP gathers with a total line length of ~ 26.5 km was chosen for the processing. Seismic reflection data were acquired in a 2D marine survey carried out in 1988 on behalf of ARCO (later acquired by BP). An airgun generated the seismic signal at 6 m depth. The shotpoint spacing was 25 m. A 240-channel streamer with 3000 m active length and 250 m lead-in with hydrophones towed at 7.5 m water depth was used. The receiver group spacing was 12.5 m. The acquisition geometry leads to 6.25 m of CMP spacing and a maximum CMP fold of 60. The record length was 7 s with 4 ms sample rate. No well information was available. The stacking velocities were determined from CRS attributes of the

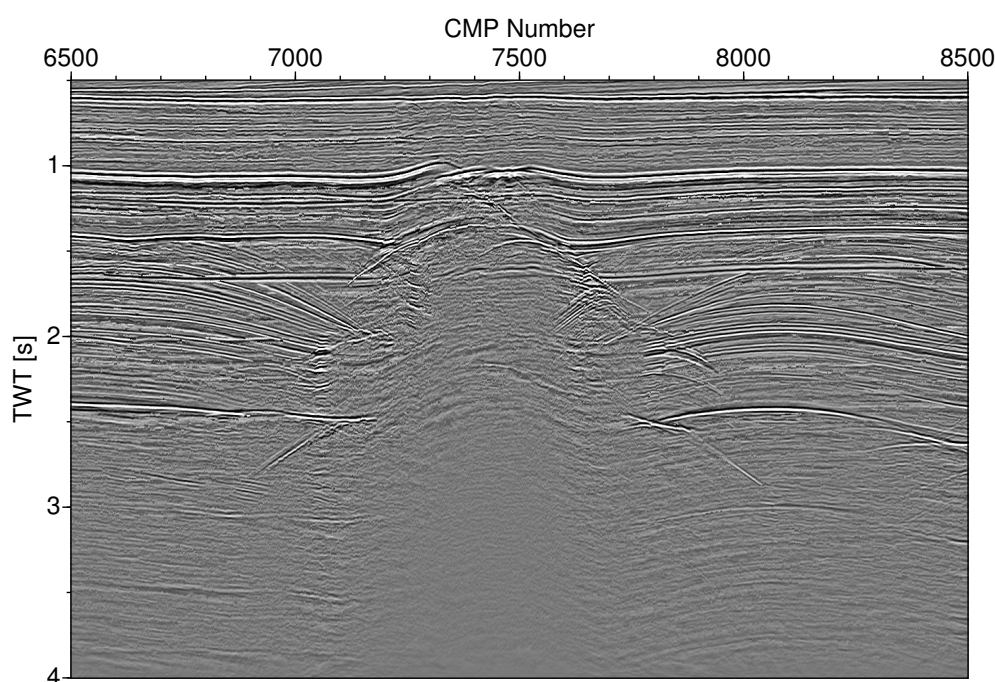


Figure 11: Marine data from the North Sea, automatic CRS stack.

data set and were used as the time migration velocities. The CSP data mapping as well as the prestack time migration was performed with these velocities. Velocity analysis of the CSP and CMP gathers was done using conventional semblance technique. The higher semblance value indicates an improved velocity analysis (Fig. 12). Figure 11 shows the prestack time migrated section (b) and the CRS stack section of CSP gathers (c). Neither for the time migrated section nor for the CRS stack any filters were applied. The reflections appear more continuous in the CRS stack section of CSP gathers compared to the prestack time migrated section, especially the top of salt and flanks of the salt appear more crisp.

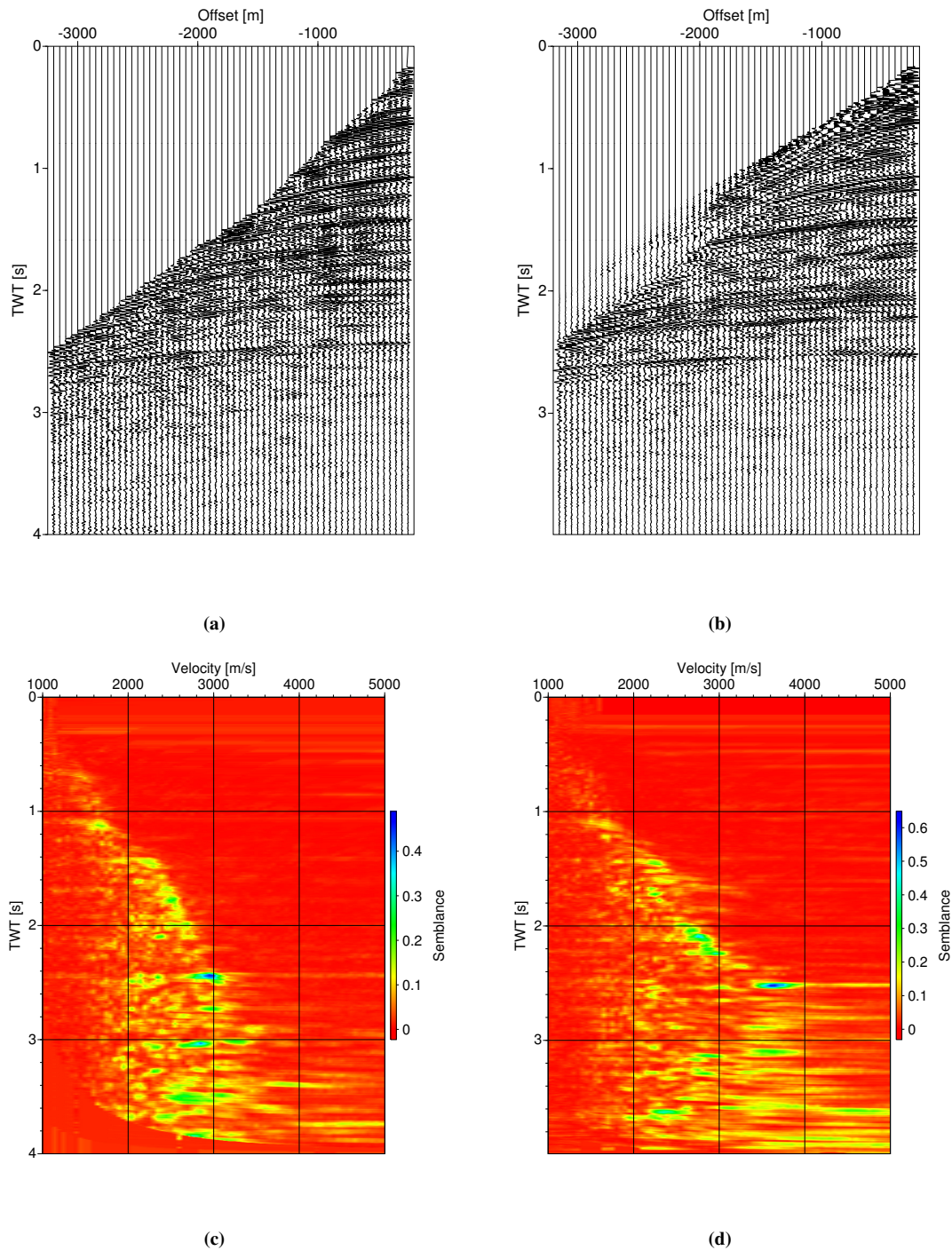
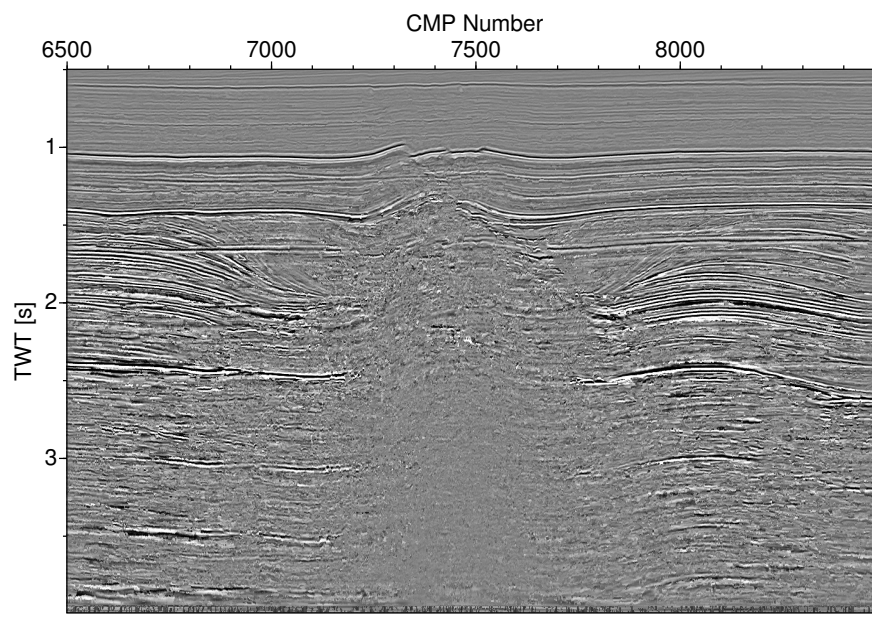


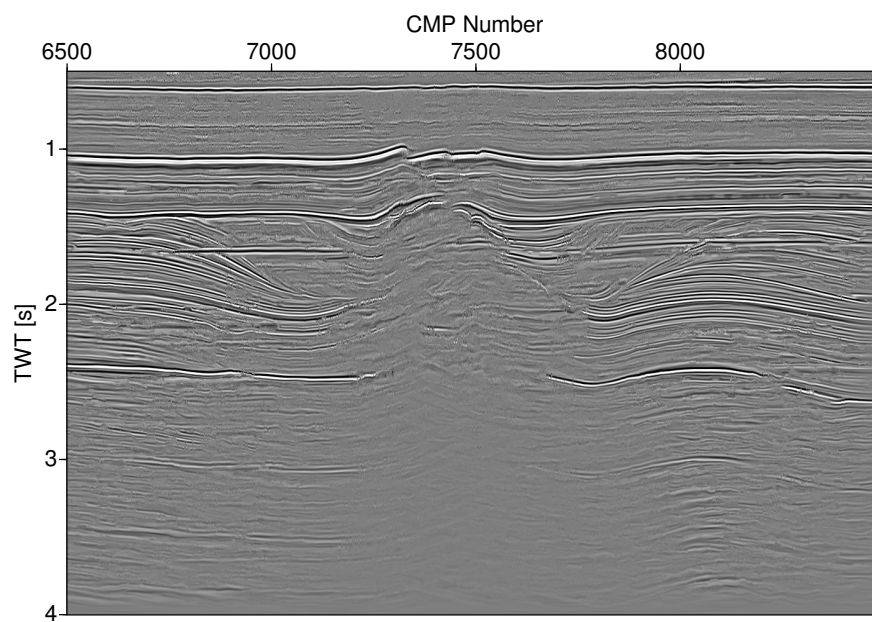
Figure 12: Marine data from the North Sea. CMP gather (a) and corresponding CSP gather (b). Velocity spectra of the CMP gather (c) and of the CSP gather (d.)

CONCLUSIONS

We have developed a method, that allows to map CMP gathers into CSP gathers. The CSP data mapping is based on the principles of Kirchhoff time migration and uses the parameterization of the DSR equation with the apex time. The summed amplitude is directly mapped into the CO apex of the migration operator.



(a)



(b)

Figure 13: Marine data from the North Sea. Automatic CRS stack of the mapped data (b) and prestack time migrated section (a). Reflections appear more continuous and the salt-sediments boundaries are easier to identify in the CRS stack section of CSP data compared to the time migrated stack section.

A CSP gather collects all scattered energy from a 3-D array (m,h,t) within the migration aperture and redistributes this energy into a 2-D array (h,t) along a hyperbolic path. When a scatter point is exactly at the output location of a CSP gather its scattered energy is constructively stacked along this hyperbolic path. Energy from scatter points displaced from the output location is canceled through destructive interference. The time domain formulation of the data mapping allows CSP gathers to be formed at arbitrary locations, i.e., a regularized gather is obtained. Also the method can be extended to 3-D geometries in a straight forward way.

Velocity analysis of the CSP gathers uses conventional semblances technique. Due to the regular geometry of these gathers and the absence of diffractions the velocity analysis is improved. We have shown that the new workflow using CSP data mapping and CRS stack provides enhanced images in comparison to the conventional prestack time migration. Reflections appear more continuous. Top of salt, flanks of salt bodies and also faults appear more crisp.

We have introduced a new workflow which includes three steps: an automatic CMP stack of the data to estimate an initial velocity model, the CSP data mapping to generate the CSP gathers from the input CMP gathers and CRS stack of CSP gathers. We have shown that the new workflow provides enhanced images in comparison to the conventional PreSTM. For complex synthetic model as well as for field data reflections appear more continuous. Top of salt, flanks of salt bodies and also faults appear more crisp.

ACKNOWLEDGMENTS

We thank the Applied Geophysics Group Hamburg for continuous discussion. The authors would like to thank the WIT consortium for the financial support. We are grateful to Stefan Dümmling, Mikhail Baykulov and Martin Tygel for discussions. We also would like to thank TGS-NOPEC and RWE Dea AG (Hamburg) for kindly providing the field data sets.

REFERENCES

- Bancroft, J., Geiger, H., and F., M. G. (1998). The equivalent offset method of prestack time migration. *Geophysics*, 21:2042–2053.
- Baykulov, M. and Gajewski, D. (2009). Prestack seismic data enhancement with partial Common Reflection Surface (CRS) stack. *Geophysics*, 74:V49–V58.
- Claerbout, J. F. (1985). *Imaging the Earth's Interior*. Blackwell.
- Clauzon, G., Suc, I., Gautier, F., Berger, A., and Loutre, M. (1996). Alternative interpretation of the messinian salinity crisis: controversy resolved? *Geologie*, 24(4):363–366.
- Hagedoorn, J. (1954). A process of seismic reflection interpretation. *Geophys. Prosp.*, 2:85–127.
- Mohr, M., Kukla, P. A., Urai, J. L., and Bresser, G. (2005). Multiphase salt tectonic evolution in NW Germany: seismic interpretation and retro-deformation. *Int J Earth Sci (Geol Rundsch)*, 94:917–940.
- Netzeband, G. L., Hübscher, C. P., and Gajewski, D. (2006). The structural evolution of the Messinian evaporites in the Levantine Basin. *Marine Geology*, 230:249–273.
- Schleicher, J., Tygel, M., and Hubral, P. (2007). *Seismic True-Amplitude Imaging*. SEG monograph.
- Silva, R. and Wang, Y. (2002). Velocity analysis after migration. *Geophys. Prosp.*, 50:539–545.
- Spinner, M. (2007). *CRS-basierte Kirchhoff-Migration mit minimaler Apertur im Zeitbereich*. PhD thesis, TH Karlsruhe.
- Yilmaz, O. (2001). *Seismic Data Processing, Vol. I and II*. SEG, Tulsa.
- Yilmaz, O. and Claerbout, J. F. (1980). Prestack partial migration. *Geophysics*, 45:1753–1779.